Conformational changes upon gating of KirBac1.1 into an open-activated state revealed by solid-state NMR and functional assays

Reza Amani[a,1], Collin G. Borcik[a,1], Nazmul H. Khan[a], Derek B. Versteeg[a], Maryam Yekefallah[a], Hoa Q. Do[a], Heather R. Coats[a], and Benjamin J. Wylie[a,2]

[a]Department of Chemistry and Biochemistry, Texas Tech University, Lubbock, TX 79409

Edited by Ann E. McDermott, Columbia University, New York, NY, and approved December 31, 2019 (received for review August 29, 2019)

The conformational changes required for activation and K^+ conduction in inward-rectifier K^+ (Kir) channels are still debated. These structural changes are brought about by lipid binding. It is unclear how this process relates to fast gating or if the intracellular and extracellular regions of the protein are coupled. Here, we examine the structural details of KirBac1.1 reconstituted into both POPC and an activating lipid mixture of 3:2 POPC:POPG (wt/wt). KirBac1.1 is a prokaryotic Kir channel that shares homology with human Kir channels. We establish that KirBac1.1 is in a constitutively active state in POPC:POPG bilayers through the use of real-time fluorescence quenching assays and Förster resonance energy transfer (FRET) distance measurements. Multidimensional solid-state NMR (SSNMR) spectroscopy experiments reveal two different conformers within the transmembrane regions of the protein in this activating lipid environment, which are distinct from the conformation of the channel in POPC bilayers. The differences between these three distinct channel states highlight conformational changes associated with an open activation gate and suggest a unique allosteric pathway that ties the selectivity filter to the activation gate through interactions between both transmembrane helices, the turret, selectivity filter loop, and the pore helix. We also identify specific residues involved in this conformational exchange that are highly conserved among human Kir channels.

solid-state NMR | potassium channel | allostery | lipid activation | membrane protein

Multiple stimuli dictate membrane protein (MP) behaviors, impacting the mutual interactions between intracellular, transmembrane, and extracellular regions of MPs. Thus, it is disappointing that the dynamic structures of MPs are often elusive. It is unknown what functional relationships exist within inward-rectifier K^+ (Kir) channels (1–7). Kir channels are grouped by their preference to pass inward K^+ current into the cell (8, 9). They maintain resting membrane potentials, regulate cell excitability, and create multiple channelopathies (10). The tetrameric Kir channel fold (Fig. 1) (11–13) includes an "inverted teepee" transmembrane structure (14) that comprises two transmembrane helices: the outer (TM1) and inner (TM2) helices. Other structural elements include a pore helix, selectivity filter (Fig. 1), and a turret located between TM1 and the pore helix. The selectivity filter loop (SFL) connects the pore helix to TM2 and contains the selectivity filter. All Kir channels possess an intracellular gating bundle, or Kir domain, which, in concert with the slide helix, responds to gating ligands, including anionic lipids, ATP, G proteins, and primary alcohols, to open the channel (8). Unlike voltage-gated K^+ (Kv) channels, Kir channels do not undergo C-type inactivation (15), and they are rectified via a voltage-dependent block by cations including Mg^{2+} and polyamines (16).

Two modes of gating exist in Kir channels. Regions near the inner gate/bundle crossing regulate slow gating, where single-channel K^+ recordings appear in bursts followed by periods of inactivity (17–19). Regions in and near the selectivity filter govern fast gating, during which K^+ current fluctuates during the slow bursts (19–24). However, the dynamic structures governing each gating process are largely unknown. Thus, improved understanding of protein–lipid interactions and the global motions associated with K^+ conduction are required to ascertain the mode and mechanism of Kir channel function.

The identification of Kir channel active states historically relies upon the confluence of X-ray crystallographic structures (1, 7, 11) or cryo-electron microscopy (EM) models (25) with functional measurements (26, 27), molecular dynamics (MD) (28, 29), and Förster resonance energy transfer (FRET) measurements (2–4, 30). However, multiple open states with different activities persist in vivo, yet structural techniques often capture discrete conformations of the protein. Capture of open-activated states often requires intelligently designed protein mutants and not wildtype protein (7). Hints to the existence of different open Kir channel states are present in the literature, including conformations that may modulate the Kir selectivity filter. These states may produce the bursts and periods of low conduction observed by electrophysiology (8).

In this work, we present a study of the archetypal Kir channel KirBac1.1 (11). The millisecond to microsecond dynamics of KirBac1.1 in detergent micelles were previously reported in a

Significance

Inward rectifier K^+ (Kir) channels play an important role in reestablishing the resting membrane state of the action potential of excitable cells in humans. KirBac1.1 is a prokaryotic Kir channel with a high degree of homology to human Kir channels and can be isotopically labeled in NMR quantities for structural studies. Functional assays and NMR assignments confirm that KirBac1.1 is in a constitutively conductive state. Solid-state NMR assignments further reveal alternate conformations at key sites in the protein that are well conserved through human Kir channels, hinting at a possible allosteric network between channels. These underlying sequential and structural motifs could explain abnormal conductive properties of these channels fundamental to their native gating processes.

Author contributions: B.J.W. designed research; R.A., C.G.B., N.H.K., D.B.V., M.Y., and B.J.W. performed research; R.A., C.G.B., N.H.K., D.B.V., M.Y., H.Q.D., H.R.C., and B.J.W. contributed new reagents/analytic tools; R.A., C.G.B., N.H.K., D.B.V., M.Y., and B.J.W. analyzed data; and R.A., C.G.B., and B.J.W. wrote the paper.

The authors declare no competing interest.

This article is a PNAS Direct Submission.

Data deposition: Chemical shift assignments have been deposited in the Biological Magnetic Resonance Bank, http://www.bmrb.wisc.edu/ (accession nos. 50123 and 50135).

[1]R.A. and C.G.B. contributed equally to this work.

[2]To whom correspondence may be addressed. Email: benjamin.j.wylie@ttu.edu.

This article contains supporting information online at https://www.pnas.org/lookup/suppl/doi:10.1073/pnas.1915010117/-/DCSupplemental.

First published January 24, 2020.

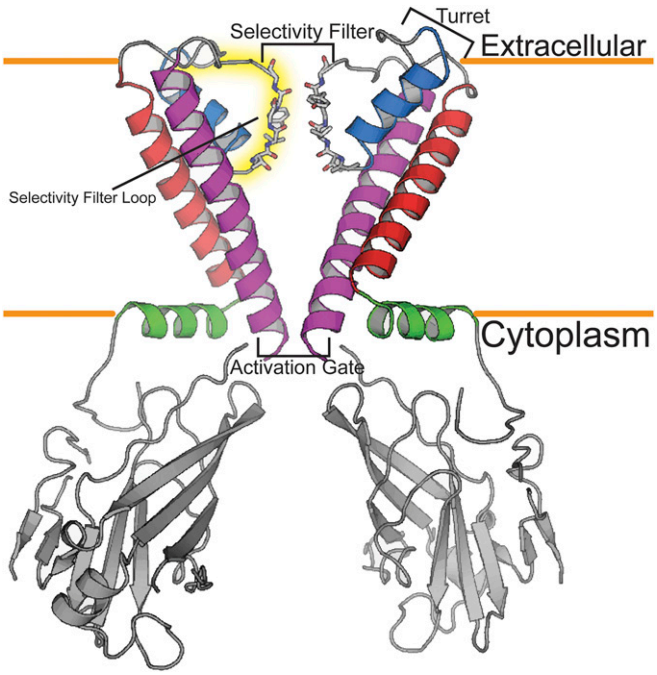

Fig. 1. Anatomy of KirBac1.1. The transmembrane portion of each monomer of KirBac1.1 is composed of four helices: slide helix (green), transmembrane helix 1 (red), pore helix (blue), and transmembrane helix 2 (magenta). The activation gate, most importantly F146, is located at the base of the inner membrane leaflet. The Kir domain, a β-sheet–rich gating bundle, protrudes into the cell cytoplasm. Regions near the top of this domain interact with anionic lipids to actuate channel gating.

liquid-state NMR study (31). This prokaryotic K^+ channel structure shares key structural elements with human Kir channels (11, 26, 27) (Fig. 1), including the selectivity filter. This selectivity filter allows K^+ to pass into the cell near the rate of free diffusion. KirBac1.1 shares ∼50% homology with eukaryotic Kir channels, including the Kir1, Kir2, and Kir3 families. There is no structure of the activated state of KirBac1.1 because activation occurs only in the presence of anionic lipids (26, 27, 32, 33) and this interaction cannot be recreated in a crystalline environment. MD (29) and FRET (2–4, 30) studies reveal multiple open states and suggest that ligand-dependent conformers of the selectivity filter may exist (4).

The conductive state of the KirBac1.1 selectivity filter is not observed in the X-ray crystal structure. Unlike many other K^+ channel structures, the crystallographic coordinates of KirBac1.1 contains only three K^+ binding sites and not the four required for K^+ conductance via the "knock-on" mechanism (34–36). Also, unlike other K^+ channel structures, the B factors for each ion occupancy site are unequal, with the S2 site possessing the greatest order. This might result from the presence of channel-rectifying Mg^{2+} in the crystallization buffer. This cation can bind to the base of the selectivity filter, perturb the S3 site, and eliminate the S4 binding site. In addition, the pore helix, and thus the pore helix dipole, is misaligned from the center of the channel, which should reduce the rate of K^+ conduction. In the case of KirBac channels, a proposed allosteric network ties conformations of the cytoplasmic domain of the channel, composed of both the N terminus and C terminus, to K^+ occupancy at the selectivity filter (1). Yet, a structure of an activatory mutant of KirBac3.1 finds all four K^+ binding sites occupied (7) coincident with an open activation gate.

In this work, we employ fluorescent functional assays (4, 37–49), measurements of relative FRET efficiencies between the open and closed states of the channel (2), and detailed solid-state NMR (SSNMR) (50) chemical shift measurements to show that the dominant conformation of KirBac1.1 in 3:2 1-palmitoyl-2-oleoyl-glycero-3-phosphocholine:1-palmitoyl-2-oleoyl-sn-glycero-3phospho-(1′-rac-glycerol) (POPC:POPG) proteoliposomes is open and conductive. This conformation is distinct from a second minor conformer and the structure observed in zwitterionic POPC bilayers. The opening of the activation gate causes the extracellular turret and SFL to pivot and introduces small kinks at glycines along the inner TM2. As TM2 twists open, it contacts sites along TM1, which allows residues further along TM1 to contact the pore helix. These conformational changes may also bring the pore helical dipole into optimal alignment for K^+ conduction by establishing a hydrogen bond between a highly conserved serine in the pore helix to a transmembrane asparagine along TM1. In the dominant observed conformer, these interactions appear to stabilize the conductive conformation of the selectivity filter. However, in the minor conformation, the selectivity filter may be deformed at the S4 K^+ binding site. In contrast, only the conductive state of the selectivity filter is observed in POPC bilayers, with much greater overall signal intensity. The observed pattern of chemical shift perturbations suggests a novel allosteric pathway distinct from C-type inactivation (51–55). In our hypothetical model, the minor conformer is a shallowly inactivated state of the selectivity filter, which is similar to the Mg^{2+}-bound (and thus rectified) conformation observed in the X-ray crystal structure (11). This indicates that this filter conformation is sampled under activating conditions, explaining the phenomenon of Kir channel fast gating. This hypothesis further suggests that rectification via divalent cations at the selectivity filter results from conformational selection of this state by the divalent blocking ligand. Thus, this hypothesis could tie rectification at the selectivity filter to similar conformational states responsible for the fast gating phenomenon.

Results and Discussion

KirBac1.1 Is Open and Active in POPC:POPG Bilayers. We confirmed the functional environments of our SSNMR sample conditions by measuring channel activity and gating motions in the same proteoliposome composition (Fig. 2). For each sample, we ensured only intact tetrameric KirBac1.1 was used (*SI Appendix*, Fig. S1). The I131C stability mutant (56) of KirBac1.1 was reconstituted into 3:2 POPC:POPG lipid bilayers as described in *Materials and Methods*. For each K^+ efflux assay (Fig. 2 *A* and *B*) (37), we reconstituted KirBac1.1 into proteoliposomes at a 200:3 lipid:protein ratio by mass. These proteoliposomes were then incubated with the H^+-sensitive 9-amino-6-chloro-2-methoxyacridine (ACMA) dye. After a baseline fluorescence reading, carbonyl-cyanide m-chlorophenylhydrazone (CCCP), a H^+ ionophore, was added to the mixture. CCCP draws H^+ into the liposome, initiating flux and quenching the ACMA signal. After the system reached equilibrium, we added valinomycin to determine the maximum possible K^+ uptake. As illustrated in Fig. 2*A*, 3:2 POPC:POPG activates the channel, and we observed nearly 80% of the maximum uptake of the valinomycin control. This is comparable to maximum uptake observed via $^{86}Rb^+$ uptake assays by other groups (26, 27, 31). The observed monoexponential decay curve was fit to a rate of K^+ conductance of 0.0098 ± 0.0002 s^{-1}. This rate is comparable to that observed for other K^+ channels using this assay (44). To further confirm the channel in POPC:POPG is not just exhibiting basal activity, we performed a series of assays as a function of the concentration of phosphatidylinositol 4,5-bisphosphate (PIP_2), a known inhibitor of KirBac1.1 (32, 57). We observed a near-complete reduction of K^+ current once the PIP_2 concentration rose above 3%. We then confirmed KirBac1.1 is inactive in zwitterionic POPC bilayers. Interestingly, we also found that KirBac1.1, even at low concentrations, stabilizes POPC bilayers. Repeated controls of protein-free POPC liposomes exhibited fluorescent signals indicative of

bilayer leakiness. This notion is supported by our previous work showing the strong relationship between KirBac1.1 and the lipid bilayer (*SI Appendix*, Fig. S2) (58).

We confirmed domain motions required for channel opening by measuring the change in FRET efficiency between the pure POPC:POPG state and the state in the presence of 1.25 to 5% PIP_2 (Fig. 2 *C–E*). Following Nichols et al., we bound Alexa Fluor-546 C5 maleimide/DABCYL-plus C2 maleimide (A/D) fluorescence donor and acceptor to the G249C mutant protein (2–4). The G249C mutant retains high channel activity compared to other reported mutants (2). The protein sample was passed through a GE Superdex 200 column prior to reconstitution to remove possible contaminating free FRET dyes (*SI Appendix*, Fig. S1*B*). Unlike previous FRET studies, we employed a higher overall anionic lipid composition in our membranes. Thus, as with the functional assays, we found that 3% PIP_2 was required for the maximum difference in FRET efficiency, greater than the 1.25% reported previously. The FRET efficiency changed by −0.05 between the POPE:POPG and POPE:POPG:PIP_2 samples, which is in very good agreement with Wang et al. (2) and indicates that KirBac1.1 undergoes a ∼6-Å motion in the C terminus upon gating. The overall FRET we observed is higher than the previous study, but the trend is nearly identical, indicating a conformational change corresponding to a rotation of the Kir domain (Fig. 2*E*). Our fluorescence data, in aggregate, confirm that POPG activates KirBac1.1 under our SSNMR conditions.

SSNMR Identifies Conformational Changes upon Lipid Binding. We reconstituted U-^{15}N,^{13}C-KirBac1.1 into POPC and 3:2 POPC:POPG proteoliposomes with a 1:1 lipid-to-protein ratio by mass. This is the same ratio we used previously (58) and is consistent with multiple previous studies of KcsA (53–55, 59–64). The sensitivity of these samples allowed us to acquire 2 two-dimensional (2D) dipole-assisted rotational resonance (DARR) (65) ^{13}C–^{13}C correlation spectra with 12 ms and 25 ms of mixing, an NCA SPECIFIC-CP (66) 2D, and NcaCX and NcoCX 2Ds with 25 ms and 35 ms of DARR following SPECIFIC CP, respectively. We also acquired three-dimensional (3D) NCACX, NCOCX, and CANcoCA spectra on both samples. All spectra were acquired using the Rovnyak theorem (67) for nonuniform sampling, and sampling schedules were generated by nus-tool in NMRBox (68) and are shown in *SI Appendix*, Fig. S3.

The measured spectra provided adequate resolution and signal-to-noise to assign large portions of the 148-kDa tetramer (37-kDa monomer) at intermediate B_0 field (600-MHz Larmor) in both samples. The assignment completeness is illustrated in *SI Appendix*, Fig. S4*A*, and observed chemical shift multiplicities and chemical shift perturbations (CSPs) are illustrated in Figs. 3 and 4 and *SI Appendix*, Figs. S4–S7.

Chemical shift assignments of POPC:POPG sample. For the POPC:POPG sample, key regions of the ^{15}N,^{13}C backbone walk are illustrated in *SI Appendix*, Figs. S4–S6. We first assigned chemical shifts in the POPC:POPG sample, as it should be the uncharacterized open channel conformation. During this process, we discovered two distinct and internally consistent backbone walks (chemical shift assignment pathways) between the end of the slide helix and the base of TM2: examples are illustrated in Fig. 3 *A–D* and *SI Appendix*, Figs. S4–S6. The greatest divergence of these separate assignment pathways (and thus largest CSPs) were observed in the three glycine residues along TM2, the VG pair at the base of the pore helix, three residues at the top of the pore helix, and a unique valine–valine pair found along TM1 (Fig. 3 *E–H*). For example, we made two distinct assignments for G143, G137, and G134 and their neighboring residues along TM2. One of these glycines, G143, was proposed to be the Kir channel hinge (11). Some of the observed linewidths are broad, including V73–V72, G99–V98, G112–V111, and I138–G137, suggesting some conformational exchange on an intermediate timescale. However, overall, the

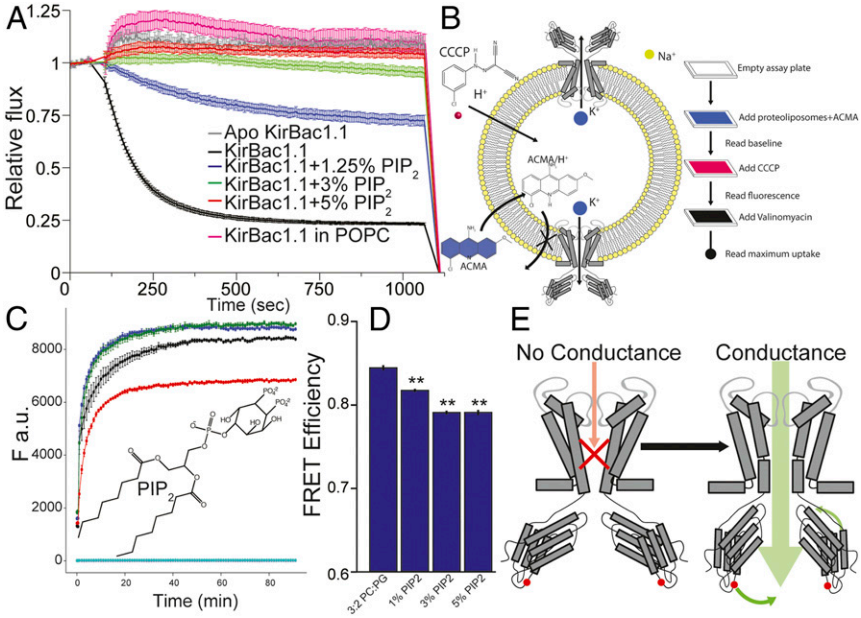

Fig. 2. K^+ flux assays confirm active channels, and FRET reveals gating motions in the C terminus upon activation. (*A*) Fluorescent monitoring of K^+ flux through the channel allows for real-time determination of the rate of flux. (*B*) Schematic outline of the K^+ fluorescence assay for rate determination. (*C*) Time-course FRET measurements from which F_{max} and F_0 measurements were obtained. Alexa Fluor-546 emission was monitored until we observed a maximum plateau. Black, POPC:POPG with A/D-labeled KirBac1.1; blue, POPC:POPG: 1.25% phosphatidylinositol 4,5-bisphosphate (PIP_2) labeled with A/D-labeled KirBac1.1; green, POPC:POPG: 3% PIP_2 labeled with A/D-labeled KirBac1.1; red, POPC:POPG: 5% PIP_2 labeled with A/D-labeled KirBac1.1, nonlabeled; magenta, POPC:POPG: nonlabeled (data are plotted behind cyan curve); cyan, POPC:POPG:PIP_2 nonlabeled. Labeled ($n = 6$) and unlabeled ($n = 3$) samples are reported as mean ± SEM. (*Inset*) Chemical structure of PIP_2 (*D*) changes in apparent FRET (mean ± SE) upon different amounts of PIP_2 in liposome. $^{**}P < 0.05$. (*E*) Cartoon of KirBac1.1 C-terminal domain motion previously reported (2) to be tied to K^+ conductance, with the red mark denoting the location of G249 in the crystal structure.

peaks appear as discrete states, suggesting two main conformations of the transmembrane region exchanging on a slow (i.e., millisecond) timescale. This slow conformational exchange timescale is consistent with microbursts observed in single-channel electrophysiology measurements previously reported for KirBac1.1 (27).

We next used our chemical shifts to determine the backbone dihedral angles ϕ and ψ using TALOS-N software (69). The dihedral angles for the dominant (red) and minor (blue) conformers are depicted in Fig. 5. Dihedral angles predicted from the X-ray crystallographic coordinates are pictured in black. The dihedral angles of both TM1 and TM2 become more regularly α-helical compared to the angles predicted by X-ray crystallography. This indicates that the helices relax and straighten into a more uniform helical structure in lipid bilayers. Second, the data indicate that TM1 is three residues longer in POPE:POPG proteoliposomes compared to the crystallographic detergent environment (residues Y81 to L84 become helical). This increased length could partially explain some of the unique features involving TM1 described here later. The B-factors from the 1P7B crystal structure are depicted in Fig. 5*A*. Many of the sites of the protein with the greatest deviation between the SSNMR-determined dihedral angles compared to X-ray are near the extracellular end of the protein, including the top of TM1, TM2, the pore helix, the selectivity filter, and the SFL. All of these structural elements have large B-factors in the 1P7B structure. These sites also exhibit significant CSPs between the major and minor conformers and have the largest error bars as determined by TALOS-N. There is a clear deviation between crystallographic angles observed in the base of the selectivity filter (T110–G112) and the angles predicted by SSNMR for the major conformer. This can be easily observed in the Ramachandran angles (*SI Appendix*, Table S2 and Fig. S11). Additionally, the RCI order parameters predicted by TALOS-N are consistent with the disorder reflected in deviations between NMR- and X-ray–derived dihedral angles and crystallographic B-factors (*SI Appendix*, Fig. S8). Interestingly, these order parameters indicate that the major conformer is slightly more ordered in the selectivity filter compared to the minor conformer, even though the preceding residues are slightly less ordered. Thus, key regions of the protein are structurally different in proteoliposomes at physiological temperature compared to crystallographic conditions.

Chemical shift assignments in POPC liposomes. We assigned the same regions of KirBac1.1 in pure POPC liposomes (Fig. 4). For ∼80% of these residues, the chemical shifts measured in a zwitterionic lipid environment are within 0.3 ppm of the assignments in POPC:POPG, confirming that the overall secondary structure of the protein is conserved. Dihedral angles predicted by TALOS-N are provided in green in Fig. 5 *B* and *C*. Notably, in POPC, the length of TM1 is identical to the crystal structure, and TM1

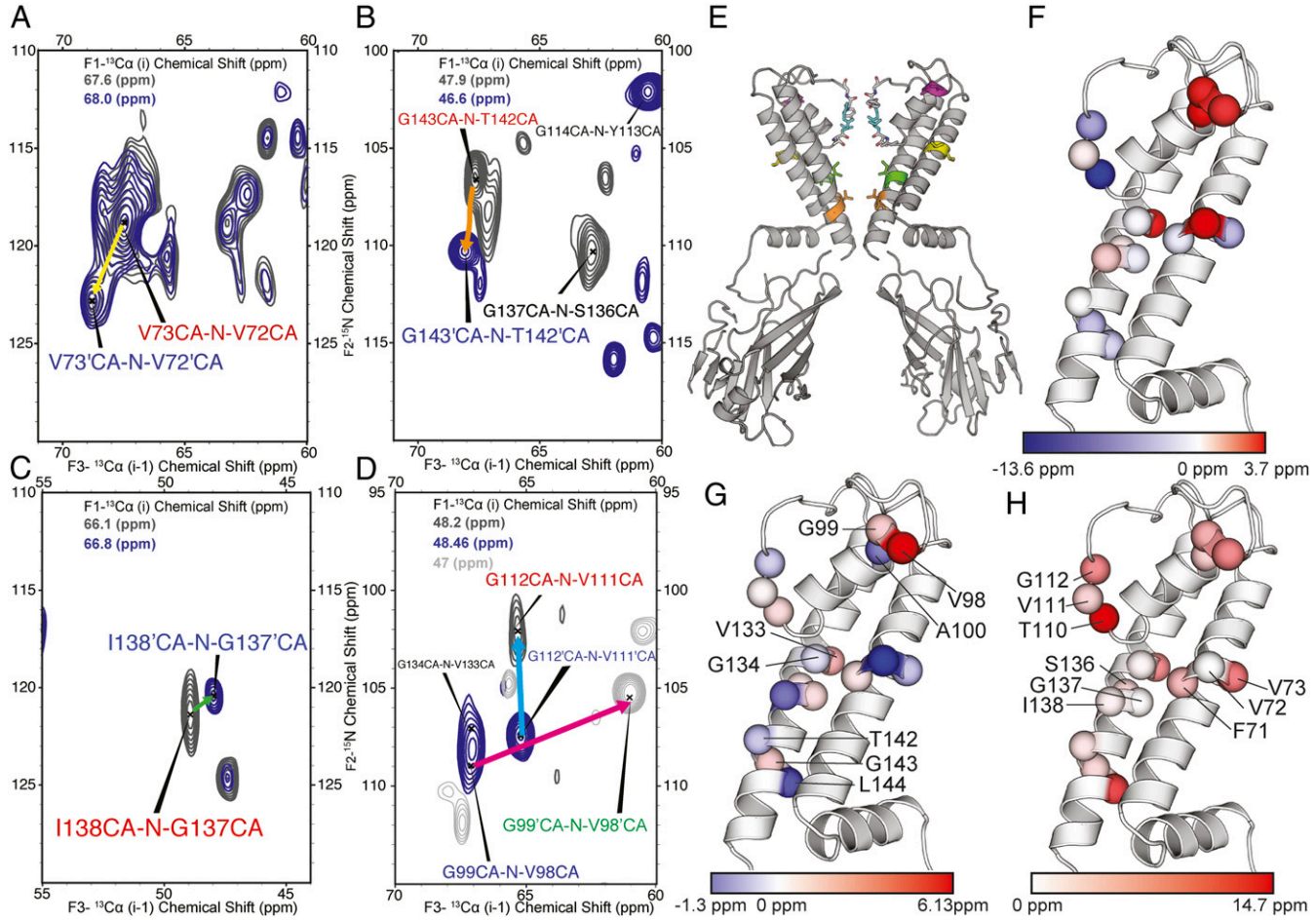

Fig. 3. CSPs of glycine and glycine-adjacent residues observed in the transmembrane region of KirBac1.1 in POPC:POPG membranes. (*A–D*) CSPs observed in the CANcoCA 3D spectra exemplifying the sensitivity to backbone rearrangements. All depicted chemical shift correlations are unique, and the perturbations cannot result from misassignment or ambiguity. (*F*) Chemical shift perturbations of the ^{15}N backbone residues mapped onto KirBac1.1 (*G*) The ^{13}Cα chemical shift perturbations. These CSPs indicate an increase in α-helical character of the dominant conductive state, which is quite striking at the top of the pore helix. (*H*) Absolute value of the sum of all CSPs indicating the global differences between the active and inactive states of the protein.

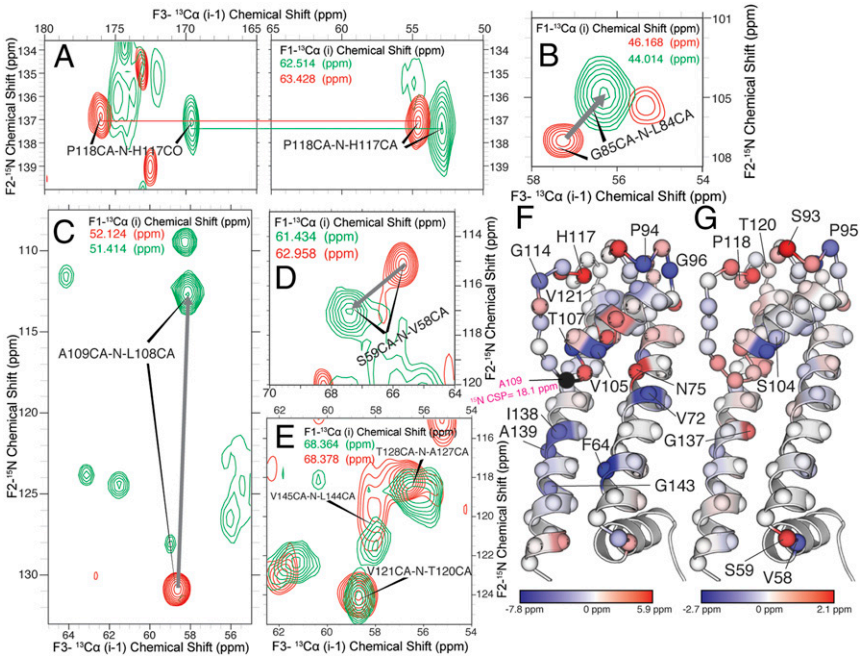

Fig. 4. Chemical shift perturbations (CSPs) between KirBac1.1 reconstituted in a zwitterionic POPC bilayer (green) and an anionic 3:2 POPC:POPG bilayer (red). (*A*–*E*) Representative assignment slices of CANcoCA 3D experiment showing (*A*) structural changes to H117–P118 at the top of the SFL, (*B*) G85–L84 at the top of TM1 showing reduced α-helical character, (*C*) significant changes in A109–L108 at the bottom of the selectivity filter, and (*D*) S59–V58 showing structural changes as a result of slide helix interactions with anionic lipids. (*E*) T120 does not respond to the lipid environment. Changes in the ^{15}N (*F*) and ^{13}Cα (*G*) chemical shifts mapped onto the structure of KirBac1.1.

terminates at Y81. Most importantly, these data revealed a third channel conformation in the perturbed regions identified earlier. Two of the largest CSPs between the third conformer and the two purported open states are observed for A109–T110 and I138–G137. The assigned peaks are strong in all POPC 3D spectra, but are completely absent from the spectra acquired in POPC:POPG. This further indicates that both observed conformers in the POPC:POPG sample correspond to an open channel, while the channel in POPC is closed (as was confirmed with the flux assay (Fig. 2), the channel is inactive and closed in POPC). In addition, several unique CSPs were found between the POPC conformation (closed conformation) and chemical shifts shared by both conformers in POPC:POPG. This third conformation deviates from the POPC:POPG conformations in the following residues: V58 and S59, V72–F78, Q83–P88, Q92–G96, V98–G99, S104–P118, Y122–I126, E130–F132, S136–A139, and T142–G143. V58 and S59 comprise the loop connecting TM1 to the slide helix. These large CSPs likely correspond to slide helix motions vital to activation. The correlations involving two of the TM2 glycine residues, G143–T142 and I138–G137, are shifted compared to both conformers observed in POPC:POPG. In aggregate, these observations indicate that both conformations identified in POPC:POPG may be open, with differing degrees of movement at each of the hinges along TM2. Throughout the POPC backbone walk, only one conformation could be cleanly identified, with the exception of the unique VV pair, V73–V72. In the X-ray crystal structure, these valine side chains face the lipid bilayer. Thus, it is possible that the structural heterogeneity found in this location is a function of specific interactions with lipid acyl chains. As stated earlier, we previously established that KirBac1.1 strongly associates with its surrounding lipids (58). As discussed later, the selectivity filter conformation in POPC is closest to the dominant conformer in POPC:POPG. Interestingly, E106, which did not display an alternate conformer population in POPC:POPG, is shifted in the POPC sample. This glutamate is known to participate in the "bow string" interactions found to stabilize the rear of the selectivity filter (60, 70, 71). An alternative pore helix-SFL orientation may also be observed in the POPC sample. The CSPs appear at both ends of the pore helix, and the largest CSP identified appears at A109 in the SFL, moving a total of 18.1 ppm in the ^{15}N dimension. This alteration to A109 could be conformationally coupled to the S4 site.

The longest stretch of contiguous CSPs found between the POPC and POPC:POPG states of the channel are located in the extracellular loops, the turret between TM1 and the pore helix, and the SFL connecting the selectivity filter to TM2. This was unexpected and may help to explain fundamental differences between Kir channels and other K^+ channel variants. In addition to small kinks along TM2, larger reorientations of the transmembrane helices may be required as critical pivot points for the channel to open. This portion of the protein may be a key player in the proposed allosteric pathways discussed later. These large conformational changes in the extracellular loops may further explain why Kir channels are less sensitive to toxin binding.

The conductive conformation of KirBac1.1. In POPC:POPG, we observed two distinct conformations of the protein. Comparison of chemical shifts measured in POPC:POPG vs. POPC (Fig. 4) suggests that both of these conformers may possess an open activation gate. It is thus possible that these two conformations correspond to an open-conductive state and an open-nonconductive state. As a first step in determining which of these proposed functional states correspond to the observed dominant channel conformation, we compared our selectivity filter chemical shift assignments to previously reported values for KcsA (Table 1). This comparison suggests that the dominant observed conformer of KirBac1.1 includes the conductive state of the selectivity filter, containing the expected S4 site required for potassium conductance. This conclusion is strongly supported by the T110 chemical shifts observed in the dominant conformer, which are strikingly close to those observed in the conductive state of KcsA. Other values along the selectivity filter are also similar to chemical shifts for the equivalent residues in KcsA, further supporting a conductive selectivity filter. The T110 chemical shifts in the minor

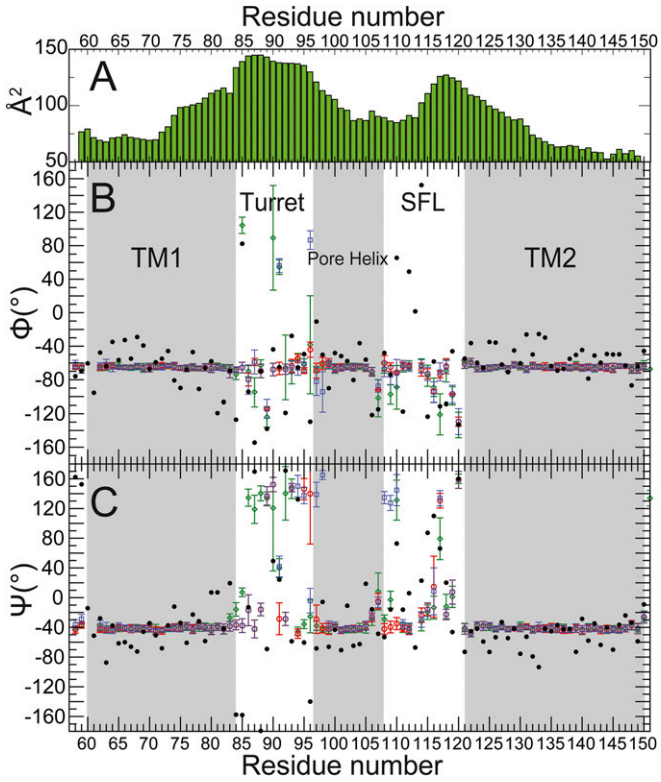

Fig. 5. Torsion angles of KirBac1.1 predicted by TALOS-N software and torsion angles from the KirBac1.1 crystal structure (PDB ID code 1P7B). (*A*) Residue-averaged B-factor per residue of the assigned portion of KirBac1.1 crystal structure. (*B* and *C*) TALOS-N predicted dihedral angles of KirBac1.1 in 3:2 POPC:POPG lipid bilayer of the major conformer (red) and the minor conformer (blue) and zwitterionic bilayer (green) versus the crystallographic dihedral angles (black).

conformer shift toward random coil values, consistent with the absence of the S4 binding site. Zhou et al. proposed that the selectivity filter undergoes structural transitions between different conformations under physiological conditions. We can support this with spectroscopic evidence of the KirBac1.1 selectivity filter transitioning between these two states (4), one of which is likely nonconductive (perhaps a "shallowly" inactive state).

We assume that the dominant KirBac1.1 population is the open-activated state of the channel. Thus, we can compare the chemical shift of each glycine along TM2 in the dominant conformation to the chemical shifts observed for glycines previously reported in KcsA in both the open and closed states of the channel. In the major conformer, ^{13}Cα chemical shifts for G137 and G143 are downfield of the peak corresponding to the minor conformation (full chemical shift listed in *SI Appendix*, Table S1), while the change in I134 (the previously proposed hinge) is small (0.2 ppm). The G137 and G143 CSPs follow the same trend as those observed in the TM2 glycine residues G99 and G104 of KcsA in the pH-activated or K^+-depleted conformation compared to the closed conformation. However, compared to the glycine chemical shifts measured in POPC, the largest change is observed at G137 (Fig. 4*G*), where chemical shifts for both the major and minor conformer are downfield of the chemical shift measured in POPC (48.9 ppm for the major protein conformer in POPC:POPG compared to 47.5 ppm observed in the POPC sample). Thus, the conformationally dependent CSPs we observed at I137 and its nearest neighbors are consistent with the pivoting and outward untwisting of this helix upon channel activation at G137, not G134. Thus, while all glycine residues are sensitive to the lipid environment, our data suggest that the true TM2 hinge is not G134, but G137. G143 may act as a minor helical kink.

The chemical shift multiplicity observed in other regions of the protein provide further clues to the structure of the open-conductive state. As stated earlier, one of the largest changes is observed in the unique V72–V73 pair, the only VV pair in KirBac1.1. The phenomenological nature of these valines experiencing different conformations far from the activation gate may be a function of both conformation and lipid association. However, in the dominant conductive conformation, sites adjacent to this VV pair, including F71, also shift. The F71 aromatic sidechain is oriented toward the cavity of KirBac1.1 in the crystal structure, facing toward G137 and I138. We hypothesize that, upon channel activation and gating, the F71 sidechain stabilizes the open conformation of the hinge at G137 and I138 by means of steric interaction via a concerted pivot motion from F71–V73.

Table 2 shows the relative populations of the two identified conformers based upon integrated intensities in the CANcoCA spectrum. We observe that the selectivity filter residues T110–V112, TM2 upper hinge G137–I138, and lower hinge G143–L144 have the greatest minor conformer populations (~40%). This could indicate that these residues act as the rate-determining sites responsible for the nonconductive state of the channel, as reflective of the maximal K^+ uptake quantity found in Fig. 2*A*. The population differences observed in the pore helix, the selectivity filter, and the hinges at G137–I138 and G143–L144 are within integration error, providing clues for possible direct influences on each relative conformation. This further supports the hypothesis that we observe two open conformers, one with a conductive selectivity filter and a second with a shallowly inactive filter (72).

Table 1. List of the conductive and the nonconductive chemical shifts of KirBac1.1 and KcsA selectivity filters

Nonconductive conformer				Conductive conformer			
KcsA resonance	Chemical shift	KirBac1.1 resonance	Chemical shift	KcsA resonance	Chemical shift	KirBac1.1 resonance	Chemical shift
T75N	113.1	T110N	124.0	T75N	108.9	T110N	109.3
T75C	172.3	T110C	172.6	T75C	172.6	T110C	172.5
T75Cα	62.5	T110Cα	62.6	T75Cα	63.2	T110Cα	63.5
T75Cβ	69.2	T110Cβ	69.3	T75Cβ	69.3	T110Cβ	69.5
V76N	116.2	V111N	120.5	V76N	119.9	V111N	120.8
V76C	175.6	V111C	178.2	V76C	178.9	V111C	179.3
V76Cα	65.2	V111Cα	65.2	V76Cα	66.2	V111Cα	65.4
V76Cβ	30.2	V111Cβ	31.3	V76Cβ	31.8	V111Cβ	33.4
G77N	104.5	G112N	107.5	G77N	99.12	G112N	102.2
G77C	173.7	G112C	175.6	G77C	174.5	G112C	175.1
G77Cα	47.2	G112Cα	48.5	G77Cα	48.7	G112Cα	48.2

Selectivity Filter-Activation Gate Allostery. As previously stated, Kir channels do not undergo slow inactivation. However, they can undergo fast gating and are rectified by cations under membrane depolarization. Recent studies show that there are fast dynamics within selectivity filters, and the "snug fit" model may be inaccurate. Thus, while it is clear that many Kir channels will crystalize with a closed activation gate and conductive selectivity filter, the B-factors in this region are relatively large. Thus, the allostery observed in this manuscript could act to transition the selectivity filter between two states. A similar allosteric coupling pathway was also identified by the Henzler-Wildman laboratory in the nonselective cation channel NaK. There, they found that NaK exhibits long-range allostery through the selectivity filter and the channel scaffolding as a result of cation passage through the channel (73). Their findings, together with ours, suggest that this behavior may be a common feature within ion channels to tightly control channel function. Thus, unlike inactivating Kv channels and KcsA, where the closed-conductive and open-nonconductive states are favored, Kir channels are unique in that channel allostery creates an equilibrium between conductive and shallowly inactive conformers. This could lead to several interesting possibilities. In the first instance, the presence of the shallowly inactivated conformer explains the fast gating phenomenon. It is thus also possible that this state is synonymous with channel rectification at the selectivity filter, and thus Kir channel blockage by divalent cations results from conformational selection rather than induced fit. It is also possible that other bilayer interactions play a role. For example, the diffusion of gating lipids could cause fluctuations in channel conformations. It is possible that this network is unique to KirBac1.1, but, based upon homology, some of these features may still be conserved in other Kir channels, including those found in humans.

Pore Helix Conformation Is Correlated to the Presence of the S4 K^+ Binding Pocket. Three large CSPs are observed at the top of the pore helix between the proposed active and inactive states: V98, G99, and A100. The $^{13}C\alpha$ chemical shifts for all three residues in the dominant conformer shift downfield, indicating increased α-helical character. This could indicate a tightening of the pore helix around its long axis. In comparison with the POPC data, the turret and SFL, which should govern the orientation of the pore helix, also shift. This may indicate a motion that brings the pore helix into proper alignment, but our data cannot definitively confirm this reorientation. This proposed reorientation of the pore helix could be stabilized by S104 forming a hydrogen bond with N75. N75 is found in an energetically unfavorable hydrophobic location within the bilayer; thus, the formation of a hydrogen bond with the close neighbor S104 could be favored. This is further supported by the apparent conformational heterogeneity in the S104 $^{13}C\alpha$ and ^{15}N peak in the CANcoCA spectrum between the POPC:POPG sample (*SI Appendix*, Fig. S10, red) and the POPC-only sample (*SI Appendix*, Fig. S10, green). N75 is directly adjacent to the F71–V73 region already shown to be related to gating motions. The pore helix of KirBac1.1 also contains multiple bulky conserved aromatic residues F101, F102, and F103. The proposed rotation of the pore helix appears correlated to the aforementioned changes in residues near the S4 K^+ binding site at the base of the selectivity filter: T110, V111, and G112. Pore helix conformational changes have been a heretofore understudied aspect of Kir channels. Literature has reported the importance of pore helix residues on the C- type activation of Kv channels (74, 75), and this has recently been investigated in KcsA (76).

Table 2. Relative populations of the major conformer of KirBac1.1 chemical shifts

Backbone residue	Population, %	Error in calculated population
V73-V72	74	±7
G99-V98	56	±10
V111-T110	56	±3
G112-V111	61	±2
G134-V133	67	±9
I138-G137	59	±2
G143-T142	64	±3
L144-G143	63	±3

Error was determined from RMS of the peak fit of the CANcoCA peak position for each conformer. The method for error quantification is presented in *SI Appendix*.

Sequential Alignment of Kir Channels Reveals a Conserved Allosteric Pathway for K^+ Gating. To further understand the observed CSP patterns and their relationship to general Kir channel dynamic structure, we performed amino acid sequential alignment of KirBac1.1 with major human Kir channel families. This analysis uncovered a possible conserved Kir channel allosteric activation model. Specifically, we found a high degree of homology between sites that possess chemical shift multiplicity and residues found in human Kir channels (Fig. 6*B*). For example, Kir channel pore helix residues exhibit similarity between species and likely retain similar selectivity filter regulatory mechanisms. In the pore helix, a conserved alanine is followed by three conserved large bulky hydrophobic residues, followed by a serine in most cases. It is our hypothesis that these aromatic residues are responsible for maintaining the integrity of the pore helix and stabilize the rear of the selectivity filter when the pore helix is positioned for optimal K^+ conduction. This then allows for the hydrogen bond donor S104 to make contact with the hydrogen bond acceptor N75 in KirBac1.1. For human Kir channels, instead of the asparagine, the hydrogen bond acceptor is the Nε of a tryptophan sidechain. E106 in the slide helix, corresponding to E71 in KcsA, forms a bowstring with D115 (70). Several KcsA studies, including recent detailed SSNMR investigations of modal gating (71), have focused upon the interactions between this pore helix glutamate and its nearest neighbors. Unlike eukaryotic Kv channels, this glutamate is conserved in most mammalian Kir channels, further indicating that the pore helix involvement we observe is common to Kir channel physiology (Fig. 6). Thus, the proposed allostery may be native to multiple Kir channels and universal to Kir channel function. A100 is also highly conserved among all Kir channels, yet the residue preceding it varies among amino acid residues with a small sidechain. In the pore helix, after the conserved A, we identified three residues following the motif F-X-F, where X is generally some bulky hydrophobic residue, often nonaromatic. Additionally, polar residues that should rarely be found in the bilayer are reliably found in these Kir sequences along the TM1 helix next to the residues equivalent to the pivotal V72 and V73, suggesting some functional role to justify their positioning close to the center of the bilayer (77, 78).

Conclusion

We have described structural changes in KirBac1.1 that coincide with a well-optimized gating environment. K^+ flux measurements demonstrate that KirBac1.1 is in an active state in the 3:2: POPC:POPG lipid bilayer and is in an inactive state in a pure POPC lipid bilayer. FRET measurements further confirmed that KirBac1.1 experiences domain motions of the cytoplasmic C-terminal domain upon activation in the same lipid environment. Detailed SSNMR chemical-shift assignments of ^{13}C-^{15}N–labeled KirBac1.1 in this same lipid environment have been correlated to distinct conformations of the protein. Based upon chemical shift assignments, we identify a predominant conformational state of KirBac1.1 that is correlated to both a conductive selectivity filter and an open activation gate. This network runs along TM2, the

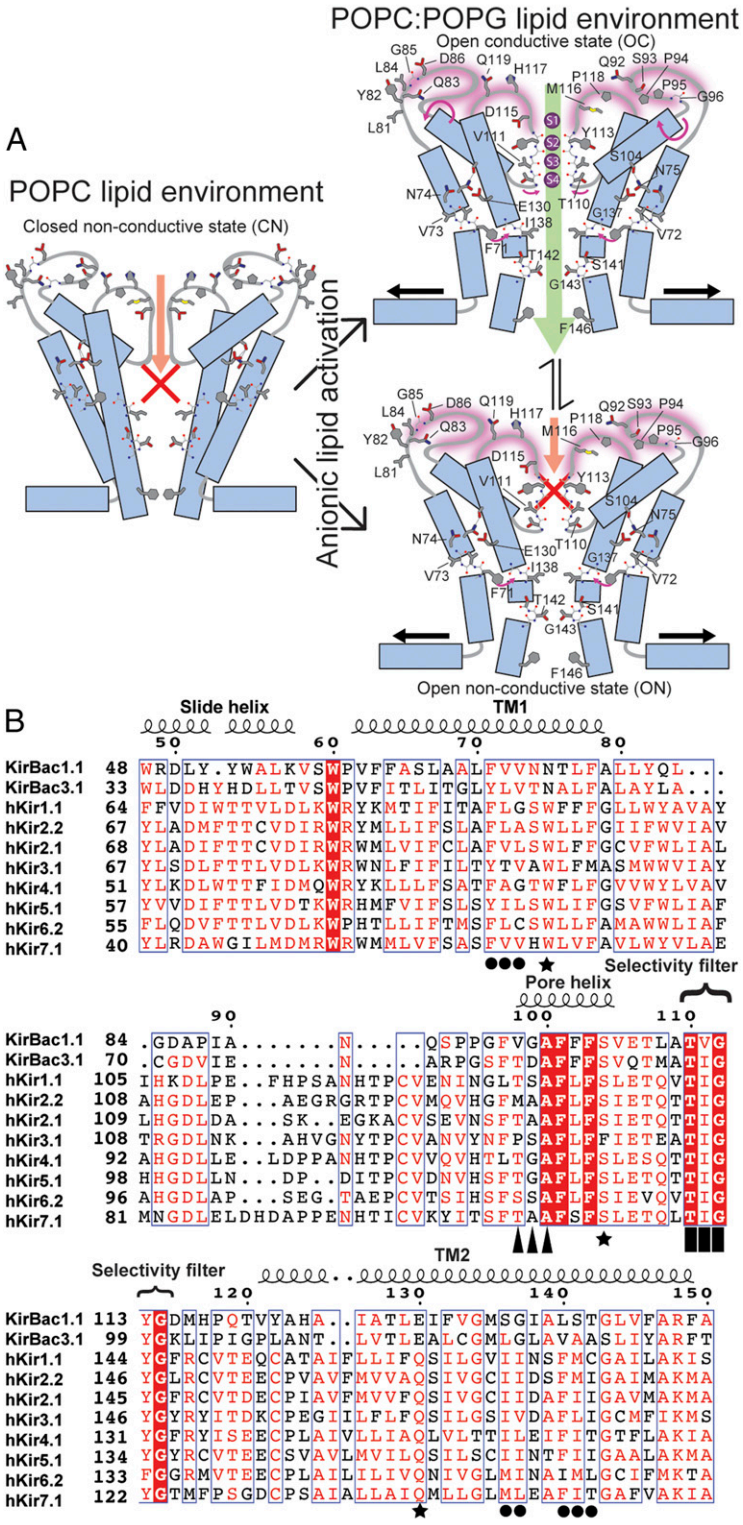

Fig. 6. Cartoon of the proposed allosteric mechanism for KirBac1.1's gating/inactivation hypothesis and sequential alignment of KirBac1.1 to human Kir channels. (*A*) Structural changes in KirBac1.1's fold resulting from anionic lipid binding. Opening the activation gate introduces slow transitions between open-conductive and open-nonconductive states of the channel. These states may be related to fast gating and rectification phenomena. (*B*) Sequential alignment of KirBac1.1 illustrating conserved homology between KirBac1.1 and human Kir channels. Circles denote the TM1 and TM2 hinge residues. Stars denote the residues potentially responsible for stabilizing rotation of the pore helix through hydrogen bonding. Triangles show residues at the start of the pore helix that are implicated in rotation of the pore helix. Rectangles are residues at the bottom of the pore helix that may move to reestablish the S4 site.

turret, the SFL, and the slide helix, and impacts TM1. We have additionally identified that KirBac1.1 goes through a structural rearrangement between the "conductive and nonconductive" states previously predicted (4), and this transition is hypothetically related to both fast gating and channel rectification at the selectivity filter. We further show, based upon homology, that some of these same allosteric features could exist in human Kir channels.

In conclusion, SSNMR assignments and measurements of CSPs have illuminated key regions in KirBac1.1 that undergo conformational rearrangements as a result of gating and activation of the channel. The regions identified herein are shared across many vital Kir channels that have been implicated in a wide variety of channelopathies and diseased states. Further work is required to explicitly calculate the changes to dihedral angles, helical alignment, and distances as a result of dynamic rearrangement upon gating. Additionally, site-specific mutagenesis of identified residues along TM1, TM2, and the pore helix could shed further light upon the exact role of each of these residues in the allosteric mechanism of K^+ conductance.

Materials and Methods

KirBac1.1 was expressed in either natural abundance or ^{15}N,^{13}C-enriched minimal media as we described previously (58). K^+ efflux assays followed the protocol of the MacKinnon laboratory as described in the main text and *SI Appendix, SI Materials* (37). All FRET measurements were conducted on a Biotek Synergy Neo2 fluorescent plate reader (Biotek Instruments) following the protocol of Wang et al. (2). Efflux and FRET data were normalized and processed using Microsoft Excel and plotted with xmgrace software. All SSNMR experiments were carried out on a 600-MHz Agilent DD2 spectrometer. NMR data were processed using NMRpipe (79) and assigned using NMRFAM-SPARKY software. Dihedral angle calculations were calculated using TALOS-N (69) software. Crystal structure dihedral angles were obtained using the SPARTA (80) software package on the KirBac1.1 crystal structure (PDB ID code 1P7B). Sequential alignment was conducted using sequences found in the UniProt database and aligned using Clustal Omega Web app (81). Additional details of experiments and data are given in *SI Appendix, SI Methods*.

Data Availability. Chemical shifts assignments have been deposited at the Biological Magnetic Resonance Bank (BMRB). The BMRB ID number for the POPC:POPG assignments is 50123 (82); for POPC assignments, the number is 50135 (83).

ACKNOWLEDGMENTS. We thank Chad Rienstra and his group for help with VNMR-J pulse programming and Colin Nichols for his gift of the I131C KirBac1.1 plasmid used in this work. We also thank Marella Canny for assistance with protein purification and sample optimization. Funding sources: This research was supported by the National Institutes of Health (Maximizing Investigators' Research Award [MIRA] R35, 1R35GM124979) and Texas Tech University Startup Funds.

1. O. B. Clarke *et al*., Domain reorientation and rotation of an intracellular assembly regulate conduction in Kir potassium channels. *Cell* **141**, 1018–1029 (2010).
2. S. Wang, S. J. Lee, S. Heyman, D. Enkvetchakul, C. G. Nichols, Structural rearrangements underlying ligand-gating in Kir channels. *Nat. Commun.* **3**, 617 (2012).
3. S. Wang, R. Vafabakhsh, W. F. Borschel, T. Ha, C. G. Nichols, Structural dynamics of potassium-channel gating revealed by single-molecule FRET. *Nat. Struct. Mol. Biol.* **23**, 31–36 (2016).
4. S. Wang *et al*., Potassium channel selectivity filter dynamics revealed by single-molecule FRET. *Nat. Chem. Biol.* **15**, 377–383 (2019).
5. W. Coyote-Maestas, Y. He, C. L. Myers, D. Schmidt, Domain insertion permissibility-guided engineering of allostery in ion channels. *Nat. Commun.* **10**, 290 (2019).
6. S. J. Lee *et al*., Structural basis of control of inward rectifier Kir2 channel gating by bulk anionic phospholipids. *J. Gen. Physiol.* **148**, 227–237 (2016).
7. V. N. Bavro *et al*., Structure of a KirBac potassium channel with an open bundle crossing indicates a mechanism of channel gating. *Nat. Struct. Mol. Biol.* **19**, 158–163 (2012).
8. H. Hibino *et al*., Inwardly rectifying potassium channels: Their structure, function, and physiological roles. *Physiol. Rev.* **90**, 291–366 (2010).
9. C. G. Nichols, A. N. Lopatin, Inward rectifier potassium channels. *Annu. Rev. Physiol.* **59**, 171–191 (1997).
10. M. R. Abraham, A. Jahangir, A. E. Alekseev, A. Terzic, Channelopathies of inwardly rectifying potassium channels. *FASEB J.* **13**, 1901–1910 (1999).
11. A. Kuo *et al*., Crystal structure of the potassium channel KirBac1.1 in the closed state. *Science* **300**, 1922–1926 (2003).
12. M. Nishida, M. Cadene, B. T. Chait, R. MacKinnon, Crystal structure of a Kir3.1-prokaryotic Kir channel chimera. *EMBO J.* **26**, 4005–4015 (2007).
13. S. B. Hansen, X. Tao, R. MacKinnon, Structural basis of PIP_2 activation of the classical inward rectifier K^+ channel Kir2.2. *Nature* **477**, 495–498 (2011).
14. Y. Zhou, J. H. Morais-Cabral, A. Kaufman, R. MacKinnon, Chemistry of ion coordination and hydration revealed by a K+ channel-Fab complex at 2.0 A resolution. *Nature* **414**, 43–48 (2001).
15. J. G. McCoy, C. M. Nimigean, Structural correlates of selectivity and inactivation in potassium channels. *Biochim. Biophys. Acta* **1818**, 272–285 (2012).
16. A. N. Lopatin, E. N. Makhina, C. G. Nichols, Potassium channel block by cytoplasmic polyamines as the mechanism of intrinsic rectification. *Nature* **372**, 366–369 (1994).
17. S. Trapp, P. Proks, S. J. Tucker, F. M. Ashcroft, Molecular analysis of ATP-sensitive K channel gating and implications for channel inhibition by ATP. *J. Gen. Physiol.* **112**, 333–349 (1998).
18. S. J. Tucker *et al*., Molecular determinants of KATP channel inhibition by ATP. *EMBO J.* **17**, 3290–3296 (1998).
19. B. A. Yi, Y. F. Lin, Y. N. Jan, L. Y. Jan, Yeast screen for constitutively active mutant G protein-activated potassium channels. *Neuron* **29**, 657–667 (2001).
20. H. Choe, H. Sackin, L. G. Palmer, Permeation properties of inward-rectifier potassium channels and their molecular determinants. *J. Gen. Physiol.* **115**, 391–404 (2000).
21. H. Choe, H. Sackin, L. G. Palmer, Gating properties of inward-rectifier potassium channels: Effects of permeant ions. *J. Membr. Biol.* **184**, 81–89 (2001).
22. D. Enkvetchakul, G. Loussouarn, E. Makhina, S. L. Shyng, C. G. Nichols, The kinetic and physical basis of K(ATP) channel gating: Toward a unified molecular understanding. *Biophys. J.* **78**, 2334–2348 (2000).
23. L. Guo, Y. Kubo, Comparison of the open-close kinetics of the cloned inward rectifier K^+ channel IRK1 and its point mutant (Q140E) in the pore region. *Receptors Channels* **5**, 273–289 (1998).
24. P. Proks, C. E. Capener, P. Jones, F. M. Ashcroft, Mutations within the P-loop of Kir6.2 modulate the intraburst kinetics of the ATP-sensitive potassium channel. *J. Gen. Physiol.* **118**, 341–353 (2001).
25. A. Kuo, C. Domene, L. N. Johnson, D. A. Doyle, C. Vénien-Bryan, Two different conformational states of the KirBac3.1 potassium channel revealed by electron crystallography. *Structure* **13**, 1463–1472 (2005).
26. D. Enkvetchakul *et al*., Functional characterization of a prokaryotic Kir channel. *J. Biol. Chem.* **279**, 47076–47080 (2004).
27. W. W. Cheng, D. Enkvetchakul, C. G. Nichols, KirBac1.1: It's an inward rectifying potassium channel. *J. Gen. Physiol.* **133**, 295–305 (2009).
28. C. Domene, A. Grottesi, M. S. Sansom, Filter flexibility and distortion in a bacterial inward rectifier K^+ channel: Simulation studies of KirBac1.1. *Biophys. J.* **87**, 256–267 (2004).
29. T. Linder, S. Wang, E. M. Zangerl-Plessl, C. G. Nichols, A. Stary-Weinzinger, Molecular dynamics simulations of KirBac1.1 mutants reveal global gating changes of Kir channels. *J. Chem. Inf. Model.* **55**, 814–822 (2015).
30. E. E. Sadler, A. N. Kapanidis, S. J. Tucker, Solution-based single-molecule FRET studies of K(+) channel gating in a lipid bilayer. *Biophys. J.* **110**, 2663–2670 (2016).
31. Y. Toyama, M. Osawa, M. Yokogawa, I. Shimada, NMR method for characterizing microsecond-to-millisecond chemical exchanges utilizing differential multiple-quantum relaxation in high molecular weight proteins. *J. Am. Chem. Soc.* **138**, 2302–2311 (2016).
32. D. Enkvetchakul, I. Jeliazkova, J. Bhattacharyya, C. G. Nichols, Control of inward rectifier K channel activity by lipid tethering of cytoplasmic domains. *J. Gen. Physiol.* **130**, 329–334 (2007).
33. W. Cheng, "From bacteria to human Biophysical studies of inward rectifying potassium channels," PhD dissertation, Washington University, Saint Louis, MO (2012).
34. S. Bernèche, B. Roux, Energetics of ion conduction through the K+ channel. *Nature* **414**, 73–77 (2001).
35. A. L. Hodgkin, R. D. Keynes, Active transport of cations in giant axons from Sepia and Loligo. *J. Physiol.* **128**, 28–60 (1955).
36. A. L. Hodgkin, R. D. Keynes, The potassium permeability of a giant nerve fibre. *J. Physiol.* **128**, 61–88 (1955).
37. Z. Su, E. C. Brown, W. Wang, R. MacKinnon, Novel cell-free high-throughput screening method for pharmacological tools targeting K+ channels. *Proc. Natl. Acad. Sci. U.S.A.* **113**, 5748–5753 (2016).
38. K. A. Kozek *et al*., Discovery and characterization of VU0529331, a synthetic small-molecule activator of homomeric G protein-gated, inwardly rectifying, potassium (GIRK) channels. *ACS Chem. Neurosci.* **10**, 358–370 (2019).
39. P. M. Riegelhaupt, G. R. Tibbs, P. A. Goldstein, HCN and K_{2P} channels in anesthetic mechanisms research. *Methods Enzymol.* **602**, 391–416 (2018).
40. L. Pope *et al*., Protein and chemical determinants of BL-1249 action and selectivity for K_{2P} channels. *ACS Chem. Neurosci.* **9**, 3153–3165 (2018).
41. I. S. Chen, Y. Kubo, Ivermectin and its target molecules: Shared and unique modulation mechanisms of ion channels and receptors by ivermectin. *J. Physiol.* **596**, 1833–1845 (2018).
42. W. Wang, R. MacKinnon, Cryo-EM structure of the open human Ether-à-go-go-related K^+ channel hERG. *Cell* **169**, 422–430.e10 (2017).
43. M. Lolicato *et al*., $K_{2P}2.1$ (TREK-1)-activator complexes reveal a cryptic selectivity filter binding site. *Nature* **547**, 364–368 (2017).
44. I. W. Glaaser, P. A. Slesinger, Dual activation of neuronal G protein-gated inwardly rectifying potassium (Girk) channels by cholesterol and alcohol. *Sci. Rep.* **7**, 4592 (2017).

45. S. Gill *et al*., A high-throughput screening assay for NKCC1 cotransporter using nonradioactive rubidium flux technology. *Assay Drug Dev. Technol.* **15**, 167–177 (2017).
46. P. K. Dadi *et al*., Selective small molecule activators of TREK-2 channels stimulate dorsal root ganglion c-fiber nociceptor two-pore-domain potassium channel currents and limit calcium influx. *ACS Chem. Neurosci.* **8**, 558–568 (2017).
47. I. S. Chen, M. Tateyama, Y. Fukata, M. Uesugi, Y. Kubo, Ivermectin activates GIRK channels in a PIP_2 -dependent, $G_{\beta\gamma}$ -independent manner and an amino acid residue at the slide helix governs the activation. *J. Physiol.* **595**, 5895–5912 (2017).
48. P. S. Shen *et al*., The structure of the polycystic kidney disease channel PKD2 in lipid nanodiscs. *Cell* **167**, 763–773.e11 (2016).
49. M. L. Garcia, G. J. Kaczorowski, Ion channels find a pathway for therapeutic success. *Proc. Natl. Acad. Sci. U.S.A.* **113**, 5472–5474 (2016).
50. B. J. Wylie, H. Q. Do, C. G. Borcik, E. P. Hardy, Advances in solid-state NMR of membrane proteins. *Mol. Phys.* **114**, 3598–3609 (2016).
51. L. G. Cuello *et al*., Structural basis for the coupling between activation and inactivation gates in K(+) channels. *Nature* **466**, 272–275 (2010).
52. L. G. Cuello, V. Jogini, D. M. Cortes, E. Perozo, Structural mechanism of C-type inactivation in K(+) channels. *Nature* **466**, 203–208 (2010).
53. B. J. Wylie, M. P. Bhate, A. E. McDermott, Transmembrane allosteric coupling of the gates in a potassium channel. *Proc. Natl. Acad. Sci. U.S.A.* **111**, 185–190 (2014).
54. Y. Xu, M. P. Bhate, A. E. McDermott, Transmembrane allosteric energetics characterization for strong coupling between proton and potassium ion binding in the KcsA channel. *Proc. Natl. Acad. Sci. U.S.A.* **114**, 8788–8793 (2017).
55. Y. Xu, D. Zhang, R. Rogawski, C. M. Nimigean, A. E. McDermott, Identifying coupled clusters of allostery participants through chemical shift perturbations. *Proc. Natl. Acad. Sci. U.S.A.* **116**, 2078–2085 (2019).
56. S. Wang, Y. Alimi, A. Tong, C. G. Nichols, D. Enkvetchakul, Differential roles of blocking ions in KirBac1.1 tetramer stability. *J. Biol. Chem.* **284**, 2854–2860 (2009).
57. D. Enkvetchakul, I. Jeliazkova, C. G. Nichols, Direct modulation of Kir channel gating by membrane phosphatidylinositol 4,5-bisphosphate. *J. Biol. Chem.* **280**, 35785–35788 (2005).
58. C. G. Borcik, D. B. Versteeg, B. J. Wylie, An inward-rectifier potassium channel coordinates the properties of biologically derived membranes. *Biophys. J.* **116**, 1701–1718 (2019).
59. M. P. Bhate *et al*., Preparation of uniformly isotope labeled KcsA for solid state NMR: Expression, purification, reconstitution into liposomes and functional assay. *Protein Expr. Purif.* **91**, 119–124 (2013).
60. M. P. Bhate, B. J. Wylie, L. Tian, A. E. McDermott, Conformational dynamics in the selectivity filter of KcsA in response to potassium ion concentration. *J. Mol. Biol.* **401**, 155–166 (2010).
61. E. A. van der Cruijsen *et al*., Importance of lipid-pore loop interface for potassium channel structure and function. *Proc. Natl. Acad. Sci. U.S.A.* **110**, 13008–13013 (2013).
62. M. Weingarth *et al*., Structural determinants of specific lipid binding to potassium channels. *J. Am. Chem. Soc.* **135**, 3983–3988 (2013).
63. C. Ader *et al*., Coupling of activation and inactivation gate in a K+-channel: Potassium and ligand sensitivity. *EMBO J.* **28**, 2825–2834 (2009).
64. C. Ader *et al*., A structural link between inactivation and block of a K+ channel. *Nat. Struct. Mol. Biol.* **15**, 605–612 (2008).
65. K. Takegoshi, S. Nakamura, T. Terao, C-13-H-1 dipolar-assisted rotational resonance in magic-angle spinning NMR. *Chem. Phys. Lett.* **344**, 631–637 (2001).
66. M. Baldus, A. Petkova, J. Herzfeld, R. Griffin, Cross polarization in the tilted frame: Assignment and spectral simplification in heteronuclear spin systems. *Mol. Phys.* **95**, 1197–1207 (1998).
67. M. R. Palmer *et al*., Sensitivity of nonuniform sampling NMR. *J. Phys. Chem. B* **119**, 6502–6515 (2015).
68. M. W. Maciejewski *et al*., NMRbox: A resource for biomolecular NMR computation. *Biophys. J.* **112**, 1529–1534 (2017).
69. Y. Shen, F. Delaglio, G. Cornilescu, A. Bax, TALOS+: A hybrid method for predicting protein backbone torsion angles from NMR chemical shifts. *J. Biomol. NMR* **44**, 213–223 (2009).
70. M. P. Bhate, A. E. McDermott, Protonation state of E71 in KcsA and its role for channel collapse and inactivation. *Proc. Natl. Acad. Sci. U.S.A.* **109**, 15265–15270 (2012).
71. S. Jekhmane *et al*., Shifts in the selectivity filter dynamics cause modal gating in K^+ channels. *Nat. Commun.* **10**, 123 (2019).
72. C. Eichmann, L. Frey, I. Maslennikov, R. Riek, Probing ion binding in the selectivity filter of the KcsA potassium channel. *J. Am. Chem. Soc.* **141**, 7391–7398 (2019).
73. J. B. Brettmann, D. Urusova, M. Tonelli, J. R. Silva, K. A. Henzler-Wildman, Role of protein dynamics in ion selectivity and allosteric coupling in the NaK channel. *Proc. Natl. Acad. Sci. U.S.A.* **112**, 15366–15371 (2015).
74. M. D. Perry, C. A. Ng, J. I. Vandenberg, Pore helices play a dynamic role as integrators of domain motion during Kv11.1 channel inactivation gating. *J. Biol. Chem.* **288**, 11482–11491 (2013).
75. G. Pages *et al*., Structure of the pore-helix of the hERG K(+) channel. *Eur. Biophys. J.* **39**, 111–120 (2009).
76. M. L. Renart *et al*., Conformational plasticity in the Kcsa potassium channel pore helix revealed by Homo-Fret studies. *Sci. Rep.* **9**, 6215 (2019).
77. L. J. Sperling *et al*., Solid-state NMR study of a 41 kDa membrane protein complex DsbA/DsbB. *J. Phys. Chem. B* **117**, 6052–6060 (2013).
78. M. Tang *et al*., Structure of the disulfide bond generating membrane protein DsbB in the lipid bilayer. *J. Mol. Biol.* **425**, 1670–1682 (2013).
79. F. Delaglio *et al*., NMRPipe: A multidimensional spectral processing system based on UNIX pipes. *J. Biomol. NMR* **6**, 277–293 (1995).
80. Y. Shen, A. Bax, SPARTA+: A modest improvement in empirical NMR chemical shift prediction by means of an artificial neural network. *J. Biomol. NMR* **48**, 13–22 (2010).
81. F. Madeira *et al*., The EMBL-EBI search and sequence analysis tools APIs in 2019. *Nucleic Acids Res.* **47**, W636–W641 (2019).
82. R. Amani, Backbone 13C, and 15N chemical shift assignments for KirBac1.1. Biological Magnetic Resonance Data Bank. http://www.bmrb.wisc.edu/data_library/summary/index.php?bmrbId=50123. Deposited 19 December 2019.
83. R. Amani, B. Wylie, KirBac1.1_POPC. Biological Magnetic Resonance Data Bank. http://www.bmrb.wisc.edu/data_library/summary/index.php?bmrbId=50135. Deposited 19 December 2019.